Atmos. Meas. Tech. Discuss., 7, 5095–5115, 2014
www.atmos-meas-tech-discuss.net/7/5095/2014/
doi:10.5194/amtd-7-5095-2014

Atmospheric Measurement Techniques Discussions
Open Access

Benefit of depolarization ratio at $\lambda = 1064$ nm for the retrieval of the aerosol microphysics from lidar measurements

J. Gasteiger and V. Freudenthaler

Meteorologisches Institut, Ludwig-Maximilians-Universität, München, Germany

Received: 17 April 2014 – Accepted: 24 April 2014 – Published: 22 May 2014

Correspondence to: J. Gasteiger (josef.gasteiger@lmu.de)

Published by Copernicus Publications on behalf of the European Geosciences Union.

Abstract

A better quantification of aerosol microphysical and optical properties is required to improve the modelling of aerosol effects on weather and climate. This task is methodologically demanding due to the huge diversity of aerosol composition and of their shape and size distribution, and due to the complexity of the relation between the microphysical and optical properties. Lidar remote sensing is a valuable tool to gain spatially and temporally resolved information on aerosol properties. Advanced lidar systems provide sufficient information on the aerosol optical properties for the retrieval of important aerosol microphysical properties. Recently, the mass concentration of transported volcanic ash, which is relevant for the flight safety of airplanes, was retrieved from measurements of such lidar systems in Southern Germany. The relative uncertainty of the retrieved mass concentration was on the order of ±50 %.

The present study investigates improvements of the retrieval accuracy when the capability of measuring the linear depolarization ratio at 1064 nm is added to the lidar setup. The lidar setups under investigation are based on the setup of MULIS and POLIS of the LMU in Munich which measure the linear depolarization ratio at 355 nm and 532 nm with high accuracy. By comparing results of retrievals applied to simulated lidar measurements with and without the depolarization at 1064 nm it is found that the availability of 1064 nm depolarization measurements reduces the uncertainty of the retrieved mass concentration and effective particle size by a factor of about 2–3. This significant improvement in accuracy is the result of the increased sensitivity of the lidar setup to larger particles. However, the retrieval of the single scattering albedo, which is relevant for the radiative transfer in aerosol layers, does hardly benefit from the availability of 1064 nm depolarization measurements.

AMTD
7, 5095–5115, 2014

1 Introduction

The microphysical properties of aerosol particles are described by their size, shape, and composition. Knowledge about these properties is required for the application of forward models, for example, in order to quantify the aerosol effect on the radiative transfer in weather and climate models; knowledge about aerosols, however, is still rather limited (Prather et al., 2008) and their climate effect is poorly quantified. Remote sensing is one of the most important tools to gain information about aerosols. Remote sensing of aerosols detects indirect effects of aerosols, for example, light scattered by the particles into the direction of the receiver. As a consequence, microphysical aerosol properties can be obtained from remote sensing measurements only indirectly, by relating the measured light scattering properties of the particles to their microphysics. This is an inverse problem, which often poses challenges due of ill-posedness (e.g., Twomey, 1977; Nakajima et al., 1983; Müller et al., 1999; Böckmann, 2001).

In the recent decades, active remote sensing by lidar became a powerful tool for aerosol research. Early lidar systems have been described for example by Collis (1966); advanced methods and applications of the lidar technique are presented for example by Weitkamp (2005). A major advantage of lidar among the remote sensing techniques is that it is vertically resolving. Lidar systems emit very short laser pulses and detect the light that is backscattered by atmospheric constituents, allowing one to derive the backscatter coefficient β of the aerosols. In order to increase the information content of measurements, advanced aerosol lidars measure backscattering at different wavelengths, use techniques that allow for the determination of the light extinction by particles (Raman lidar and high spectral resolution lidar, see Ansmann and Müller, 2005), and measure the polarization state of the backscattered light (Sassen, 2005). Most polarization lidars emit linearly-polarized light and measure the fraction of the backscattered light that is polarized parallel to the polarization plane of the emitted laser light separately from the fraction that is polarized perpendicular to this plane (Freudenthaler et al., 2009). The linear volume depolarization ratio δ_l^V is the ratio of the

AMTD
7, 5095–5115, 2014

backscatter coefficient measured at the perpendicular channel $\beta_\perp$ to the backscatter coefficient measured at the parallel channel $\beta_\parallel$:

$$\delta_l^V = \frac{\beta_\perp}{\beta_\parallel} \tag{1}$$

Both, air molecules and aerosol particles are relevant for the backscattering from the atmosphere. The linear depolarization ratio δ_l of the aerosol particles, which is of interest for aerosol characterization, can be extracted from δ_l^V, as shown by Biele et al. (2000). Observations of the linear depolarization ratio δ_l allow one to distinguish spherical from non-spherical particles (Schotland et al., 1971) because δ_l is zero for spherical particles and larger than zero for non-spherical particles. The depolarization parameter d, as discussed by Gimmestad (2008), describes the same property as the linear depolarization ratio δ_l and a unique relationship exists between d and δ_l. d is linear in atmospheric quantities, e.g. d is equal to 0.5 if a non-depolarizing particle ($d = 0$) occurs together with a completely depolarizing particle ($d = 1$) with the same total amount of backscattering. By contrast, δ_l of such a mixture is 1/3, showing the non-linearity of δ_l with respect to particle properties. The circular depolarization ratio δ_c is also uniquely related to δ_l if the assumption that particles and mirror particles are equiprobable and in random orientation is fulfilled, which is true for most practically important cases (Mishchenko and Hovenier, 1995). In the following we accept this assumption, thus δ_l, d, and δ_c provide the same piece of information about the aerosols, and the findings of our study employing δ_l can be transferred to d and δ_c as well.

Aside from providing the potential to detect spherical particles, the linear depolarization ratio δ_l of non-spherical particles is also a function of the size parameter $x = 2\pi r/\lambda$, with r being the particle radius and λ the wavelength. This size parameter dependence is illustrated for example in Fig. 2 of Gasteiger et al. (2011b). In general, δ_l is quite low if non-spherical particles are smaller than the wavelength (in the mentioned figure $0.0 < \delta_l < 0.1$ for $x < 2$), but significantly higher if non-spherical particles are comparable or larger than the wavelength ($0.1 < \delta_l < 0.7$ for $x > 4$ and non-absorbing particles).

As a result of this size parameter dependence, δ_l of an aerosol ensemble can be wavelength-dependent and measurements of δ_l at additional wavelengths potentially increase the information content of the measurements about the particle size. Furthermore, such additions may also be useful for the characterization of other microphysical parameters because the size dependence of δ_l varies with refractive index and particle shape (Gasteiger et al., 2011b).

The combination of the advanced Raman lidar systems POLIS and MULIS (Freudenthaler et al., 2009) of the Meteorological Institute of the Ludwig-Maximilians-Universität in Munich, Germany, measures the linear depolarization ratio δ_l and the extinction coefficient α at two wavelengths ($\lambda = 355$ nm and 532 nm), and the backscatter coefficient β at three wavelengths ($\lambda = 355$ nm, 532 nm, and 1064 nm). Microphysical properties of transported volcanic ash have been retrieved using measurements from this lidar setup by means of a Monte Carlo approach in which modelled optical properties of sampled spheroid ensembles are compared to the lidar measurements (Gasteiger et al., 2011a). Relative uncertainties in the order of 50 % have been found for the particle mass concentrations and effective radii, resulting mainly from the uncertainty of the measurements; the main source of uncertainty was found to be the low sensitivity to the presence of large particles (about $r > 3$ µm). Thus, enhancements of the existing lidar systems are envisaged in order to increase the accuracy of the retrieval, and it seems natural that extensions of the setup towards larger wavelengths increase the sensitivity to the presence of large particles. In order to support decisions on cost-effective enhancements of the lidar systems, the present contribution investigates to which extent channels for the linear depolarization ratio δ_l at $\lambda = 1064$ nm, abbreviated as $\delta_{l,1064}$ in the following, can help to decrease the uncertainties associated with the microphysical retrieval. It is worth mentioning that channels for $\delta_{l,1064}$ have already been integrated in a HSR lidar of the NASA Langley Research Center (Hair et al., 2008). In the present study, retrieval results for simulated lidar measurements with different lidar setups (with and without channels for $\delta_{l,1064}$) are compared. A single aerosol ensemble is assumed in Sect. 3 to simulate the lidar measurements on which the retrieval is

AMTD
7, 5095–5115, 2014

applied. In Sect. 4 the generality of the results from Sect. 3 is verified by considering a larger set of aerosol ensembles that are used for simulating the lidar measurements.

2 Methods

The microphysical retrieval approach of Gasteiger et al. (2011a) is applied to simulated lidar measurements. We briefly summarize this retrieval approach: The Monte Carlo method is applied for random sampling of the microphysical parameters of aerosol ensembles. The ensembles consist of spheroids. The microphysics of the ensembles is described by parameters for the size distribution (log-normal), the aspect ratio distribution (modified log-normal), and the complex refractive index (wavelength-independent). The ranges of microphysical parameters covered by the retrieval are given in Table 2 of Gasteiger et al. (2011a). The optical properties of each sampled ensemble are modeled using the T-matrix method (Mishchenko and Travis, 1998) supplemented by the Geometric Optics Approach (Yang et al., 2007) for large particles not covered by the T-matrix method. The modeled optical properties of each ensemble are compared to the (simulated) lidar measurements, and those ensembles that agree with the measurements within the attributed uncertainty of the measurements are accepted as solutions of the retrieval. Finally, the property of interest, e.g. the effective radius, is calculated for each ensemble in the set of solutions, and a probability distribution for the property of interest is obtained. Ranges including 95 % of the solutions, from the 2.5 %-percentile to the 97.5 %-percentile, are denoted as (min .. max). This is the 95 % confidence interval. The uncertainties of the retrieved parameters are defined by the widths of the 95 % confidence intervals.

For the evaluation of the benefit of the linear depolarization ratio $\delta_{l,1064}$, we have to rely on simulated lidar measurements on which we apply the retrieval. In order to make the simulated lidar measurements as realistic as possible with respect to relevant aerosol types, we assume only aerosol ensembles that are compatible with the volcanic ash measurements on 17 April 2010 in Maisach. Furthermore, we assume

Discussion Paper | Discussion Paper | Discussion Paper | Discussion Paper |

AMTD

7, 5095–5115, 2014

Aerosol retrieval with depolarization at 1064 nm

J. Gasteiger and V. Freudenthaler

three different lidar setups: The first lidar setup (S1) is the lidar setup of MULIS and POLIS with the relative uncertainties of the 17 April measurements; this setup does not include $\delta_{l,1064}$. By contrast, the second (S2) and third (S3) setups include channels for $\delta_{l,1064}$, whereby the other channels are the same as in setup S1. The second and third setups differ from each other by the relative uncertainty of $\delta_{l,1064}$: the third setup S3 assumes the relative uncertainty of $\delta_{l,1064}$ to be the average of the relative uncertainties of δ_l at 355 nm and 532 nm, whereas the uncertainty of $\delta_{l,1064}$ in setup S2 is doubled compared to setup S3 in order to investigate the effect of measurement uncertainties.

The present contribution focuses on potential benefits of $\delta_{l,1064}$ for the retrieval of the effective radius r_{eff}, the mass-extinction conversion factor η, and the single scattering albedo ϖ_0, which are calculated from the sampled microphysical properties of the ensembles. The effective radius r_{eff} is defined here as

$$r_{\text{eff}} = \frac{\int r_c^3 n(r_c) \mathrm{d}r_c}{\int r_c^2 n(r_c) \mathrm{d}r_c}, \quad (2)$$

where r_c is the cross-section-equivalent radius of the particles and $n(r_c)$ the particle number density per radius interval. The effective radius r_{eff} is the cross-section-weighted average particle radius. Note that other definitions of the effective radius exist, see e.g. McFarquhar and Heymsfield (1998).

The mass-extinction conversion factor η (unit: g m^{-2}) is the ratio between the mass concentration M (unit: g m^{-3}) and the extinction coefficient α (unit: m^{-1}),

$$\eta = \frac{M}{\alpha}. \quad (3)$$

η is required for the conversion of extinction coefficients, as measured by lidar, to mass concentrations, e.g. of volcanic ash or cloud particles.

The single scattering albedo ϖ_0 is

$$\varpi_0 = \frac{\alpha_{\text{sca}}}{\alpha}, \quad (4)$$

Discussion Paper | Discussion Paper | Discussion Paper | Discussion Paper |

AMTD

7, 5095–5115, 2014

Aerosol retrieval with depolarization at 1064 nm

J. Gasteiger and V. Freudenthaler

with the scattering coefficient α_{sca} and the extinction coefficient α, thus describing the ratio between the amount of light scattered by the particles to the amount of light interacting with the particles. Interacting light that is not scattered is absorbed by the particles and usually transformed into heat. ω_0 is an important parameter for the radiative transfer in aerosol layers.

3 Results

An ensemble was randomly chosen from the ensembles that are compatible with the lidar measurements of volcanic ash on 17 April 2010 in Maisach (Gasteiger et al., 2011a). This ensemble is referred to as the "truth" in this section and its optical parameters serve as input for the retrieval. The refractive index m is $1.474 + 0.00705i$, the modal radius of the log-normal size distribution is $r_0 = 0.516\,\mu m$, and its width is $\sigma = 1.639$, which corresponds to $r_{eff} = 0.9495\,\mu m$. 71.05 % of the particles are prolate spheroids with a modified log-normal aspect ratio distribution with $\mu_p = 0.234$ and $\sigma_p = 1.253$; 28.95 % of the particles are oblate spheroids with aspect ratio distribution parameters $\mu_o = 0.405$ and $\sigma_o = 0.821$. The optical properties are summarized in Table 1. As we investigate only intensive properties, we selected an arbitrary value of $1\,km^{-1}$ for the extinction coefficient α at $\lambda = 355\,nm$. The particle mass density is assumed to be $\rho = 2.6\,g\,cm^{-3}$.

Figure 1 shows the mass-extinction conversion factors η of the retrieved ensembles over their effective radii r_{eff}. The black dots denote ensembles retrieved without consideration of $\delta_{l,1064}$ (setup S1), red and green dots show ensembles retrieved when $\delta_{l,1064}$ is considered with different measurement uncertainties (setup S2 and S3). For each setup 100 000 compatible ensembles have been retrieved. The blue cross marks the properties of the ensemble used as input for the retrieval ("truth"). Analogous to the retrieval of volcanic ash properties presented by Gasteiger et al. (2011a), η over r_{eff} of the solutions are distributed close to a straight line, indicating strong correlation between both ensemble parameters. The Pearson correlation coefficient between both

AMTD
7, 5095–5115, 2014

parameters is 0.994 for setup S1. It is obvious from Fig. 1 that the uncertainty of the retrieved η and r_{eff} decreases notably if $\delta_{l,1064}$ is considered. The 95 % confidence interval for r_{eff} is the range (0.78··2.03 µm) in case of non-consideration of $\delta_{l,1064}$ (setup S1). When $\delta_{l,1064}$ is considered with the higher uncertainty (setup S2), this range shrinks to (0.82··1.26 µm) (Table 2). Thus, the retrieval uncertainty of r_{eff} in setup S2 is reduced by a factor of 2.8 compared to setup S1. This reduction factor increases to 3.7, if the uncertainty of $\delta_{l,1064}$ is reduced (setup S3). In accordance with the almost linear relationship between η and r_{eff}, the reduction factors for the η-uncertainties are in the same range (S2 vs. S1: 2.8, S3 vs. S1: 3.6). For each setup, the 95 % confidence interval includes the r_{eff} and η of the "truth", and the medians of the solutions get closer to the "truth" if $\delta_{l,1064}$ is considered and its attributed uncertainty decreases.

The frequency of sampling compatible ensembles is reduced by a factor of 4.3 (S2) and 8.9 (S3) when $\delta_{l,1064}$ is added to the lidar setup. Figure 2 shows for the three lidar setups the frequencies of sampling compatible ensembles that fall within r_{eff} bins of 0.1 µm widths. In setups S2 and S3, $\delta_{l,1064}$ serves as an additional criterion on the compatibility of the ensembles, thus the sampling frequencies for all r_{eff} bins are lower or equal in these setups than in setup S1 (neglecting the statistical noise from the Monte Carlo sampling). The difference between the curves illustrates the effect of the consideration of $\delta_{l,1064}$ on the retrieval of r_{eff}. It primarily sorts out ensembles with large r_{eff}, whereby ensembles with $r_{eff} > 1.45$ µm (S2) and $r_{eff} > 1.31$ µm (S3) do not occur anymore.

To investigate in further detail the effect of considering $\delta_{l,1064}$, Fig. 3 shows the real parts of the refractive indices m_r over r_{eff} of the compatible ensembles. By comparing the $m_r - r_{eff}$ areas covered depending on the lidar setup it becomes clear that $\delta_{l,1064}$ primarily helps to exclude ensembles with high r_{eff} and to a far lesser extent also low m_r. The uncertainty of the retrieved real part of the refractive index m_r is reduced by a factor of 1.4 (setup S2) and 1.5 (setup S3) if $\delta_{l,1064}$ is considered (Table 2); the agreement of the median m_r with the true m_r improves. Furthermore, Table 2 shows that measurements of $\delta_{l,1064}$ exclude solutions with low imaginary part of the refractive index m_i. But the uncertainty of m_i is reduced only by a factor of 1.21 and 1.25 if $\delta_{l,1064}$ is considered (Table 2), indicating slightly higher sensitivity of $\delta_{l,1064}$ to the real part m_r than to the imaginary part m_i. This agrees well with findings of Wiegner et al. (2009), where a higher sensitivity of δ_l to changes of m_r than for changes of m_i was found for the shorter wavelength $\lambda = 532$ nm.

Figure 4 shows the frequencies of sampling compatible ensembles that fall within single scattering albedo ω_0 bins of 0.01 widths at $\lambda = 532$ nm. The consideration of $\delta_{l,1064}$ removes a large fraction of ensembles with large ω_0 but, in general, it excludes ensembles on the whole range of ω_0 (compare red and green with black boxes). The median ω_0 from setup S1 provides very good agreement with the true ω_0, whereas the agreement between median and true ω_0 becomes slightly worse if $\delta_{l,1064}$ is added to the setup (Table 2). The 95 % confidence intervals of ω_0 cover the true ω_0 for all setups. The uncertainty of the retrieved ω_0 is virtually independent of the lidar setup, which indicates that $\delta_{l,1064}$ hardly contains information on ω_0. This finding for ω_0 at $\lambda = 532$ nm is also valid for ω_0 at $\lambda = 1064$ nm (not shown).

4 Statistical verification

Only a single randomly chosen aerosol ensemble that is compatible with the volcanic ash measurements in Maisach (Gasteiger et al., 2011a) was used as input (“truth”) for the microphysical retrievals in the previous section. As other aerosol ensembles are also compatible with these measurements, the question arises whether the above findings are specific for this single ensemble or they can be generalized to other ensembles that are compatible with these ash measurements. Therefore, we investigate in this section retrievals for a larger set of input ensembles but with a smaller number of compatible output ensembles. 100 randomly chosen input ensembles that are compatible with the volcanic ash measurements are used for this purpose, and 100 compatible ensembles are retrieved for each combination of input ensemble and lidar setup. For this verification, the same lidar setups and relative uncertainties of the input

AMTD
7, 5095–5115, 2014

parameters as in the previous section are used (Table 1), but the parameter values are varied depending on the selected input ensembles. The widths of the 95 %-uncertainty ranges are calculated for each retrieval case and averaged over the 100 input ensembles in order to obtain average uncertainties of the retrieved parameters for each lidar setup.

Table 3 shows the average width of the 95 %-uncertainty ranges of the retrieved effective radius r_{eff} and single scattering albedo ϖ_0 for the three lidar setups. The average width for r_{eff} is reduced by a factor of 1.71 (setup S2) and 2.05 (setup S3) when $\delta_{\mathrm{l},1064}$ is added to the lidar setup. By contrast, the average width for the single scattering albedo ϖ_0 is reduced only by a factor of 1.09 (setup S2) and 1.11 (setup S3) if this additional channel is added. Thus, the uncertainty of r_{eff} is reduced significantly stronger than the uncertainty of ϖ_0 by adding $\delta_{\mathrm{l},1064}$ to the lidar setup. This qualitatively validates the generality of the findings from the previous section.

5 Conclusions

In a case study using a simulated aerosol measurement assuming three different lidar setups, which are based on the existing lidar systems MULIS and POLIS, we evaluated improvements that can be expected for the retrieval of microphysical properties of non-spherical aerosols from adding the capability of measuring $\delta_{\mathrm{l},1064}$, the linear depolarization ratio at $\lambda = 1064$ nm, to the lidar setup. It was found that significant improvements can be expected for the retrieval of the effective radius r_{eff} and the mass concentration M, whereas only minor improvements should be expected for the retrieval of the single scattering albedo ϖ_0. The significant improvements for r_{eff} and M are a result of the high sensitivity of $\delta_{\mathrm{l},1064}$ to the presence of large particles. The improvements are found even if the uncertainty of the δ_{l} measurements at 1064 nm is slightly higher than the uncertainty of the δ_{l} measurements at 355 nm and 532 nm. These results have been validated by a statistical analysis of the uncertainties of r_{eff} and ϖ_0 retrieved from a large set of simulated aerosol measurements.

AMTD
7, 5095–5115, 2014

J. Gasteiger and V. Freudenthaler

Though in the present study wavelength independence of the refractive index was assumed, it needs to be emphasized that the refractive index of real aerosol particles can be wavelength-dependent and vary between the particles of an ensemble. Measurements of the refractive index of mineral and volcanic particles suggest only weak spectral variation of the real part in the wavelength range of our lidars (355 nm to 1064 nm), whereas the imaginary part can vary considerably in this spectral range (see for example Wagner et al., 2012, , and references therein). Furthermore we emphasize that the estimation of the mass concentration M depends more critically on assumptions like the mass density ρ of the particles if the uncertainty about r_{eff} is reduced by consideration of $\delta_{\text{l},1064}$.

The benefits of $\delta_{\text{l},1064}$ are expected to be qualitatively comparable also for other advanced lidar systems that operate within or close to the visible spectral range. Even for simple lidar systems, such as ceilometers (Wiegner et al., 2014), the capability of measuring $\delta_{\text{l},1064}$ could be a quite useful enhancement because of its sensitivity to large non-spherical particles, such as desert dust and volcanic ash aerosols.

In summary, we have shown that channels for the linear depolarization ratio δ_{l} at $\lambda = 1064$ nm are valuable extensions of existing lidar systems for the retrieval of effective particle sizes or the mass concentration of transported volcanic ash and other aerosol types with similar r_{eff}.

Acknowledgements. This work was partly funded by the LMUexcellent project EVAeNT.

References

Ansmann, A., and Müller, D.: Lidar and Atmospheric Aerosol Particles, in: Lidar, edited by Weitkamp, C., vol. 102 of Springer Series in Optical Sciences, Springer New York, 105–141, doi:10.1007/0-387-25101-4_4, 2005. 5097

Biele, J., Beyerle, G., and Baumgarten, G.: Polarization lidar: correction of instrumental effects, Opt. Express, 7, 427–435, doi:10.1364/OE.7.000427, 2000. 5098

AMTD

7, 5095–5115, 2014

Böckmann, C.: Hybrid regularization method for the ill-posed inversion of multiwavelength lidar data in the retrieval of aerosol size distributions, Appl. Optics, 40, 1329–1342, doi:10.1364/AO.40.001329, 2001. 5097

Collis, R. T. H.: Lidar: a new atmospheric probe, Q. J. Roy. Meteor. Soc., 92, 220–230, doi:10.1002/qj.49709239205, 1966. 5097

Freudenthaler, V., Esselborn, M., Wiegner, M., Heese, B., Tesche, M., Ansmann, A., Müller, D., Althausen, D., Wirth, M., Fix, A., Ehret, G., Knippertz, P., Toledano, C., Gasteiger, J., Garhammer, M., and Seefeldner, M.: Depolarization ratio profiling at several wavelengths in pure Saharan dust during SAMUM 2006, Tellus B, 61, 165–179, doi:10.1111/j.1600-0889.2008.00396.x, 2009. 5097, 5099

Gasteiger, J., Groß, S., Freudenthaler, V., and Wiegner, M.: Volcanic ash from Iceland over Munich: mass concentration retrieved from ground-based remote sensing measurements, Atmos. Chem. Phys., 11, 2209–2223, doi:10.5194/acp-11-2209-2011, 2011a. 5099, 5100, 5102, 5104

Gasteiger, J., Wiegner, M., Groß, S., Freudenthaler, V., Toledano, C., Tesche, M., and Kandler, K.: Modeling lidar-relevant optical properties of complex mineral dust aerosols, Tellus B, 63, 725–741, doi:10.1111/j.1600-0889.2011.00559.x, 2011b. 5098, 5099

Gimmestad, G. G.: Reexamination of depolarization in lidar measurements, Appl. Optics, 47, 3795–3802, doi:10.1364/AO.47.003795, 2008. 5098

Hair, J. W., Hostetler, C. A., Cook, A. L., Harper, D. B., Ferrare, R. A., Mack, T. L., Welch, W., Izquierdo, L. R., and Hovis, F. E.: Airborne high spectral resolution Lidar for profiling aerosol optical properties, Appl. Optics, 47, 6734–6752, doi:10.1364/AO.47.006734, 2008. 5099

McFarquhar, G. M. and Heymsfield, A. J.: The definition and significance of an effective radius for ice clouds., J. Atmos. Sci., 55, 2039–2052, doi:10.1175/1520-0469(1998)055<2039:TDASOA>2.0.CO;2, 1998. 5101

Mishchenko, M. I. and Hovenier, J. W.: Depolarization of light backscattered by randomly oriented nonspherical particles, Opt. Lett., 20, 1356–1358, doi:10.1364/OL.20.001356, 1995. 5098

Mishchenko, M. I. and Travis, L. D.: Capabilities and limitations of a current Fortran implementation of the T-Matrix method for randomly oriented, rotationally symmetric scatterers, J. Quant. Spectrosc. Ra., 60, 309–324, doi:10.1016/S0022-4073(98)00008-9, 1998. 5100

Müller, D., Wandinger, U., and Ansmann, A.: Microphysical particle parameters from extinction and backscatter lidar data by inversion with regularization: theory, Appl. Optics, 38, 2346–2357, doi:10.1364/AO.38.002346, 1999. 5097

Nakajima, T., Tanaka, M., and Yamauchi, T.: Retrieval of the optical properties of aerosols from aureole and extinction data, Appl. Optics, 22, 2951–2959, doi:10.1364/AO.22.002951, 1983. 5097

Prather, K. A., Hatch, C. D., and Grassian, V. H.: Analysis of atmospheric aerosols, Annu. Rev. Anal. Chem., 1, 485–514, doi:10.1146/annurev.anchem.1.031207.113030, 2008. 5097

Sassen, K.: Polarization in Lidar, in: Lidar, edited by: Weitkamp, C., Springer Series in Optical Sciences, vol. 102, Springer New York, 19–42, doi:10.1007/0-387-25101-4_2, 2005. 5097

Schotland, R. M., Sassen, K., and Stone, R.: Observations by Lidar of linear depolarization ratios for hydrometeors, J. Appl. Meteorol., 10, 1011–1017, doi:10.1175/1520-0450(1971)010<1011:OBLOLD>2.0.CO;2, 1971. 5098

Twomey, S.: Introduction to the Mathematics of Inversion in Remote Sensing and Indirect Measurements, Dover Publications, Mineola, New York, 1977. 5097

Wagner, R., Ajtai, T., Kandler, K., Lieke, K., Linke, C., Müller, T., Schnaiter, M., and Vragel, M.: Complex refractive indices of Saharan dust samples at visible and near UV wavelengths: a laboratory study, Atmos. Chem. Phys., 12, 2491–2512, doi:10.5194/acp-12-2491-2012, 2012. 5106

Weitkamp, C. (Ed.): LIDAR: Range-Resolved Optical Remote Sensing of the Atmosphere, Springer, 2005. 5097

Wiegner, M., Gasteiger, J., Kandler, K., Weinzierl, B., Rasp, K., Esselborn, M., Freudenthaler, V., Heese, B., Toledano, C., Tesche, M., and Althausen, D.: Numerical simulations of optical properties of Saharan dust aerosols with emphasis on lidar applications, Tellus B, 61, 180–194, doi:10.1111/j.1600-0889.2008.00381.x, 2009. 5104

Wiegner, M., Madonna, F., Binietoglou, I., Forkel, R., Gasteiger, J., Geiß, A., Pappalardo, G., Schäfer, K., and Thomas, W.: What is the benefit of ceilometers for aerosol remote sensing? An answer from EARLINET, Atmos. Meas. Tech. Discuss., 7, 2491–2543, doi:10.5194/amtd-7-2491-2014, 2014. 5106

Yang, P., Feng, Q., Hong, G., Kattawar, G. W., Wiscombe, W. J., Mishchenko, M. I., Dubovik, O., Laszlo, I., and Sokolik, I. N.: Modeling of the scattering and radiative properties of nonspherical dust-like aerosols, J. Aerosol Sci., 38, 995–1014, doi:10.1016/j.jaerosci.2007.07.001, 2007. 5100

AMTD

7, 5095–5115, 2014

Aerosol retrieval with depolarization at 1064 nm

J. Gasteiger and V. Freudenthaler

Title Page
Abstract | Introduction
Conclusions | References
Tables | Figures
◀ | ▶
Back | Close
Full Screen / Esc
Printer-friendly Version
Interactive Discussion

Table 1. Simulated lidar-relevant aerosol parameters and attributed uncertainties used as input for the retrieval in Sect. 3; parameters are extinction coefficient α, backscatter coefficient β, and linear depolarization ratio δ_l; S1, S2, S3 denote the different lidar setups.

parameter	value	relative uncertainty	setup S1	setup S2	setup S3
α at $\lambda = 355$ nm	1.000 km^{-1}	±7.4 %	x	x	x
α at $\lambda = 532$ nm	1.0927 km^{-1}	±11.1 %	x	x	x
β at $\lambda = 355$ nm	0.01908 km^{-1} sr^{-1}	±5.3 %	x	x	x
β at $\lambda = 532$ nm	0.02243 km^{-1} sr^{-1}	±4.1 %	x	x	x
β at $\lambda = 1064$ nm	0.01751 km^{-1} sr^{-1}	±16.0 %	x	x	x
δ_l at $\lambda = 355$ nm	0.3571	±4.4 %	x	x	x
δ_l at $\lambda = 532$ nm	0.3687	±2.0 %	x	x	x
δ_l at $\lambda = 1064$ nm	0.3005	±6.4 %		x	
δ_l at $\lambda = 1064$ nm	0.3005	±3.2 %			x

AMTD
7, 5095–5115, 2014

Aerosol retrieval with depolarization at 1064 nm

J. Gasteiger and V. Freudenthaler

Table 2. Medians and 95 % confidence intervals (min..max) of the effective radius r_{eff}, the mass-extinction conversion factor η, the single scattering albedo ϖ_0, and the refractive index m retrieved in Sect. 3 for the three lidar setups; for comparison also the parameters of the input ensemble ("truth") are given.

parameter	setup S1	setup S2	setup S3	"truth"
r_{eff} [µm]	1.28 (0.78..2.03)	1.03 (0.82..1.26)	1.01 (0.83..1.17)	0.95
η at 532 nm [g m^{-2}]	1.55 (0.89..2.56)	1.22 (0.94..1.54)	1.19 (0.96..1.42)	1.16
ϖ_0 at 532 nm	0.896 (0.832..0.958)	0.877 (0.827..0.945)	0.875 (0.826..0.945)	0.893
m_r	1.431 (1.355..1.489)	1.457 (1.396..1.492)	1.459 (1.404..1.492)	1.474
$m_i \times 1000$	5.2 (1.3..12.7)	7.6 (3.0..12.4)	8.0 (3.1..12.3)	7.0

AMTD
7, 5095–5115, 2014

Table 3. Average width of the 95 % confidence intervals of the effective radius r_{eff} and the single scattering albedo ϖ_0 obtained from the statistical analysis using 100 input aerosol ensembles (see text for details).

parameter, average interval width of	setup S1	setup S2	setup S3
r_{eff} [µm]	1.23	0.72	0.60
ϖ_0 at $\lambda = 532$ nm	0.122	0.112	0.110

AMTD
7, 5095–5115, 2014

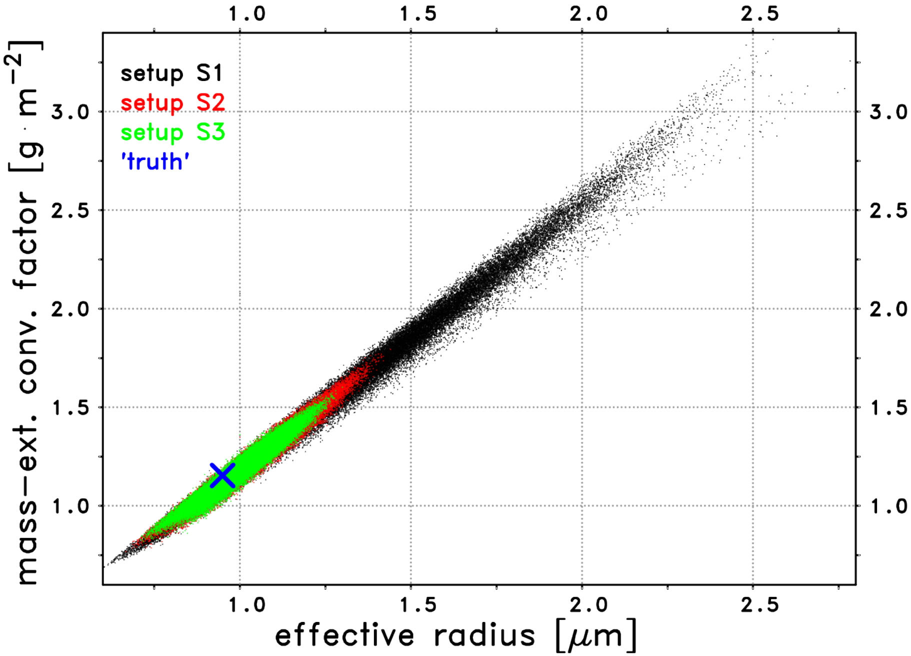

Figure 1. Mass-extinction conversion factor η at $\lambda = 532$ nm over effective radius r_{eff} of retrieved ensembles for the three lidar setups and the ensemble used as retrieval input ("truth").

AMTD
7, 5095–5115, 2014

J. Gasteiger and V. Freudenthaler

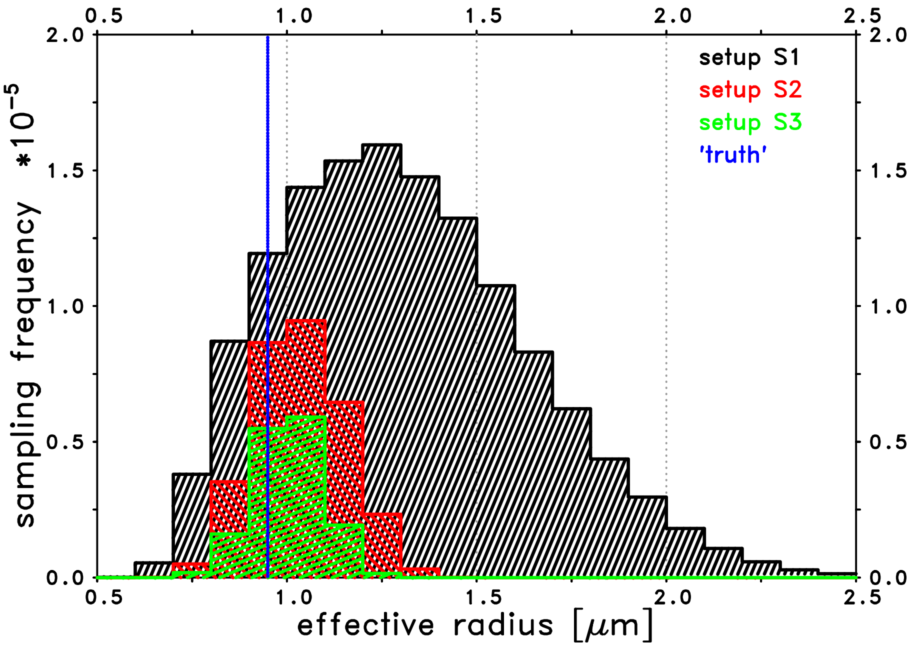

Figure 2. Sampling frequency for compatible ensembles within effective radius r_{eff} bins of 0.1 µm width; r_{eff} of the ensemble used as retrieval input ("truth") is shown as a vertical line.

AMTD
7, 5095–5115, 2014

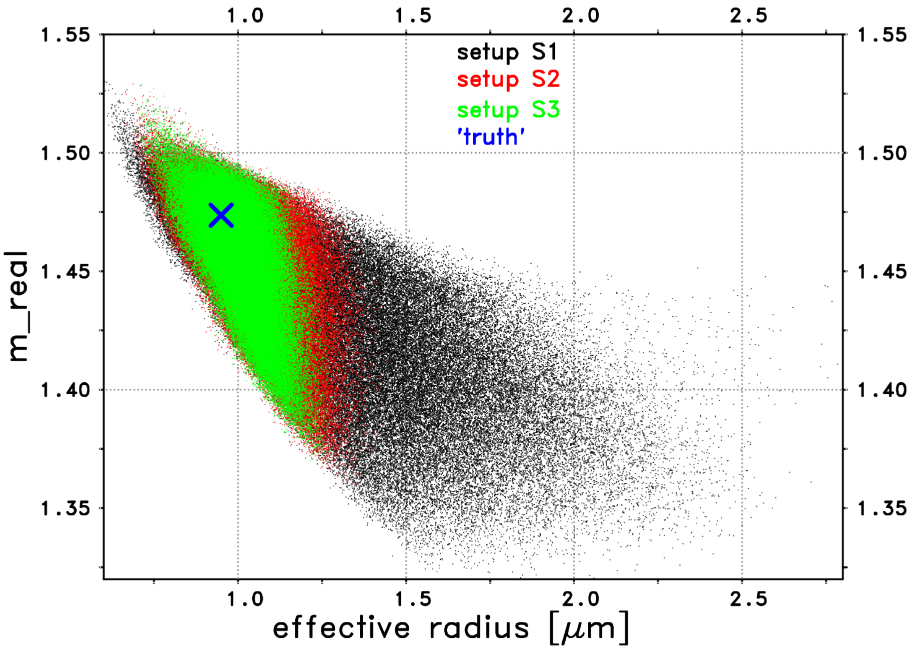

Figure 3. Real part of the refractive index m_r over effective radius r_{eff} of retrieved ensembles for the three lidar setups and the ensemble used as retrieval input ("truth").

AMTD
7, 5095–5115, 2014

Aerosol retrieval with depolarization at 1064 nm

J. Gasteiger and V. Freudenthaler

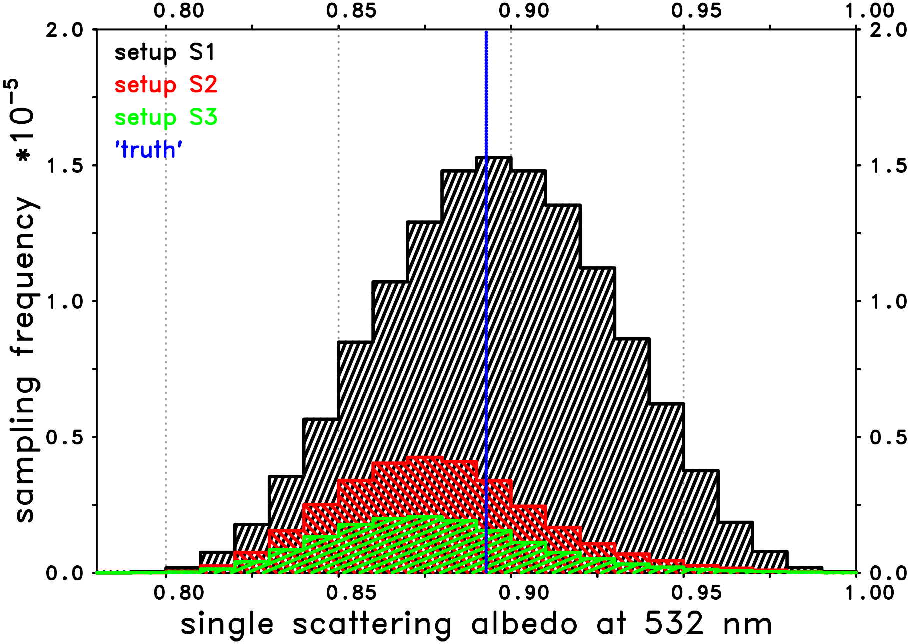

Figure 4. Sampling frequency for compatible ensembles within single scattering albedo ω_0 bins of 0.01 width at $\lambda = 532$ nm; ω_0 of the ensemble used as retrieval input ("truth") is shown as a vertical line.

AMTD
7, 5095–5115, 2014

Aerosol retrieval with depolarization at 1064 nm

J. Gasteiger and V. Freudenthaler